Journal of Information Systems Engineering and Management
2025, 10(4)
e-ISSN: 2468-4376
https://www.jisem-journal.com/

Research Article

Composite Gain-Scheduled Control Design for IPMSM Speed Regulation Using an Extended State Observer

[1]Mohanad H. K. Shehada, [2] S. Tara Kalyan

[1]PhD Student, Department of Electrical and Electronics Engineering, Jawaharlal Nehru Technological University Hyderabad, Kukatpally, Hyderabad, Telangana, India
H.T. No.:2201102001, E-mail: mohanad.moh83@gmail.com
[2]Sr. Professor, Department of Electrical and Electronics Engineering, University College of Engineering, Science & Technology Hyderabad, Jawaharlal Nehru Technological University Hyderabad, Kukatpally, Hyderabad, Telangana, India
E-mail: tarakalyani@jntuh.ac.in

ARTICLE INFO

Received: 10 May 2025
Revised: 17 May 2025
Accepted: 22 May 2025

ABSTRACT

The study presents a composite gain-scheduled control system integrated with an estimation technique based on an Extended State Observer (ESO) to enhance the robustness and tracking performance of the Interior Permanent Magnet Synchronous Motor (IPMSM) drive system under varying operating conditions. The composite control system comprises an integral state feedback controller (I-SFC) enhanced with a dynamic gain scheduling mechanism, and an extended state observer (ESO). The ESO is designed to account for the mechanical dynamics of the IPMSM and is incorporated in the speed control loop to estimate the lumped disturbance affecting the loop. The design of the scheduled controller involves approximating the nonlinear dynamic model of an IPMSM into a parameterized linear formulation that relies on scheduling variables, namely load disturbance and reference speed, to accommodate changes in linear dynamics. An integral state feedback control with a gain scheduling mechanism is then developed to regulate the linearized model. The controller regularly updates the linear model and modifies the gain settings based on current disturbance estimates and reference speed to ensure stability and accurate tracking under varying operating conditions. The effectiveness of the proposed control scheme is validated through simulation tests in the MATLAB/Simulink environment. Simulation results demonstrate that the proposed scheduled I-SFC method significantly outperforms the fixed-gain I-SFC method, particularly regarding dynamic performance and robustness to disturbances.

Keywords: Interior Permanent Magnet Synchronous Motor (IPMSM); gain-scheduled control; composite control; Extended State Observer (ESO); state feedback control; scheduling variables

1. INTRODUCTION

Permanent magnet synchronous motors (PMSMs), including surface-mounted (SPMSMs) and interior-mounted (IPMSMs) types, have received significant research interest due to their high power density, high efficiency, considerable torque capability, compact design, and broad speed range [1], [2]. These attributes make them a preferred choice for various applications, from robotics and aerospace systems, where space is limited [3], to electric vehicles that support sustainable energy mobility [2]. Despite the advantages mentioned above, the control of these motors continues to present a significant challenge due to their high nonlinearity, strong coupling among their variables, and being subject to various sources of disturbances [4].

Vector control is a widely used technique for addressing challenges related to PMSMs control. It converts three-phase currents into orthogonal d-q axis currents, enabling independent speed and torque control through a cascade control structure. This control structure comprises an outer control loop to regulate speed and inner control loops to manage currents along the d and q axes. Consequently, the PMSM can attain high dynamic capabilities comparable to DC motors, while retaining the inherent benefits of AC motor design [5].

Journal of Information Systems Engineering and Management
2025, 10(4)
e-ISSN: 2468-4376
https://www.jisem-journal.com/

Research Article

Proportional-integral (PI) controllers are commonly used for speed regulation in PMSM drives that employ vector control due to their simple structure and ease of implementation. However, these controllers exhibit restricted dynamic performance under changing conditions and external disturbances [6]. While the effects of disturbance can be managed through the integral action of the PI structure, this comes at the expense of response efficiency [7].

Disturbance estimation-based control techniques are used within the vector control framework to achieve the desired tracking performance while enhancing robustness against disturbances and uncertainties [8]. These control methods are built upon a composite architecture comprising a feedback baseline controller, disturbance estimation techniques, and a compensation mechanism. The baseline controller is designed to satisfy performance criteria, while the disturbance estimation technique is incorporated into the control structure to estimate system disturbances and uncertainty, which allows for appropriate compensation to mitigate or eliminate their adverse impacts on system performance [8], [9].

Among the well-known methods for estimating disturbances, the Disturbance Observer (DO) and the Extended State Observer (ESO) are widely used in AC drive systems [3], [8]. These techniques can provide accurate and rapid estimates of various types of disturbances, including parameter uncertainties and external load variations, as well as their overall impact, thereby enhancing performance in the presence of disturbances.

The baseline controller can be designed using nonlinear methods that address the inherent complexity of PMSMs, such as sliding mode control [7], [10] backstepping control [11], fractional PD control [12], and so on. Although nonlinear methods offer high performance in dynamic environments, their design complexity and high computational requirements may limit their practical use. Therefore, systematic linear control approaches, such as state-feedback controls, are often more appropriate in specific situations, as they can simplify design and reduce computational burden.

The dynamic model of PMSM requires linearization before implementing SFC control within the vector control framework, which can be accomplished using techniques like feedback linearization [13], or the Jacobian approximation method [14]. When SFC acts as the baseline controller, the complete system is managed by a single controller, enhancing coordination among state variables and facilitating the integration of a disturbance observer into the control structure. Moreover, it enables the adoption of the linear quadratic regulator (LQR), which improves system performance by determining optimal pole locations. However, maintaining optimal performance under changing operating conditions poses a significant challenge, as the effectiveness of the approximated model reduces under these conditions.

One effective way to extend the validity of the approximated model is to incorporate an adaptive feature based on disturbance estimates into the control structure. This adaptive attribute enables dynamic updates to the model parameters, thereby expanding its applicability to a range of operating conditions. In this regard, a disturbance observer-based sensorless speed control system integrated with a gain scheduling mechanism was introduced in [14] to enhance robustness against disturbances in the SPMSM system. The state feedback control with integral action was employed as the baseline controller, and the disturbance estimates provided by the disturbance observer (DO) were utilized to adjust the operating point, resulting in continuous updates to the linearized model and control law. Consequently, the control performance was significantly enhanced across various operating conditions.

Despite the effectiveness of the previous methodology in improving performance under different operating conditions, restricting the update of the locally model to only one scheduling variable, namely the estimated disturbance, and designing the controller based on a constant reference speed limits its adaptability to the systems that require prompt response to continuous changes in both speed and load torque, such as electric vehicle propulsion systems. Therefore, this study aims to extend the previous approach by broadening the coverage of scheduling variables to include the reference speed and estimated disturbances. Thus, it can enhance adaptability to more dynamic conditions and allow for more accurate tracking performance. Furthermore, the application scope is shifted to IPMSM, which exhibits more complex dynamics than SPMSM. This allows for the demonstration of the effectiveness of the proposed scheme under more challenging conditions and broadens its potential areas of use.

In this paper, a composite gain-scheduled control system combining an I-SFC controller, a disturbance estimation technique based on ESO, and a scheduling mechanism is introduced for vector control-based IPMSM drives to

Journal of Information Systems Engineering and Management
2025, 10(4)
e-ISSN: 2468-4376
https://www.jisem-journal.com/

Research Article

enhance dynamic speed tracking performance and robustness against disturbances. The ESO is integrated into the control structure to estimate the disturbances affecting the speed loop. During the control design process, a parametrized linear formulation for the IPMSM is developed and augmented with additional integral state equations. The scheduled I-SFC controller is then designed to regulate the augmented model through the application of the LQR optimization technique. The scheduling mechanism allows for dynamic updates of the control law based on current ESO estimates and reference speed. Therefore, the control system can adapt to continuous changes in operating conditions. The main contributions of this work can be summarized as follows:

- Formulate a parameterized linear model for IPMSM to extend the applicability of the approximated version and facilitate the development of the dynamic scheduling mechanism for control parameters.
- Develop a composite scheduled control that integrates an integral SFC controller, an ESO, and a dynamic scheduling mechanism for the speed control of IPMSM.
- Validate the effectiveness of the proposed strategy for IPMSM control system through simulation tests performed in MATLAB/Simulink under two different operating conditions.

The subsequent sections of the paper are organized as follows: Section 2 presents the mathematical model of the IPMSM drive under vector control, along with its linear approximation. Section 3 introduces the design of the composite scheduled control for the IPMSM system. Section 4 describes the validation through simulation tests and shows the findings. The final section presents conclusions and recommendations for the future.

2. MODELLING OF IPMSM UNDER VECTOR CONTROL

Developing a mathematical model for IPMSM in a three-phase stationary reference frame yields a nonlinear model characterized by time-varying parameters and coupling dynamics. The inherent complexities of the model pose obstacles to applying advanced control strategies within the original motor frame. In contrast, modeling in the rotor reference frame simplifies the dynamics and mitigates the coupling effect by transforming the time-varying parameters into constant values, thereby facilitating the application of advanced control methods.

2.1 Nonlinear mathematical modeling of IPMSM motor under vector control

The electrical and mechanical dynamics of the IPMSM in the rotating dq reference frame are governed by nonlinear equations, as presented in the following expressions [15].

$$\begin{aligned}\frac{di_d}{dt} &= -\frac{R_s}{L_d}i_d + n_p\frac{L_q}{L_d}i_q\omega_r + \frac{1}{L_d}v_d \\ \frac{di_q}{dt} &= -\frac{R_s}{L_q}i_q - n_p\frac{L_d}{L_q}i_d\omega_r - n_p\frac{\lambda_f}{L_q}\omega_r + \frac{1}{L_q}v_q \\ \frac{d\omega_r}{dt} &= \frac{3}{2}\frac{n_p}{J_m}\{\lambda_f i_q + (L_d - L_q)i_d i_q\} - \frac{B}{J_m}\omega_r - \frac{1}{J_m}T_L\end{aligned} \tag{1}$$

where v_d , v_q, i_d and i_q represent the voltages and currents in the d-q axis, respectively. The electrical coefficients R_s, L_d, and L_q represent the stator winding resistance, stator inductance along the d-axis, and stator inductance along the q-axis, respectively. The magnetic coefficient λ_f signifies permanent magnetic flux linkage. The mechanical coefficients J_m, B, and n_p denote the moment of inertia, viscous friction coefficient, and number of pole pairs, respectively. T_L, an ω_r refer to the applied load torque disturbance and mechanical rotor speed.

The dynamics of the inverter in the rotor reference frame can be approximated as a proportional element, defining the relation between the control input and the voltage applied to the motor windings as [16], [17]:

$$\begin{bmatrix} v_d \\ v_q \end{bmatrix} = K_p \begin{bmatrix} u_d \\ u_q \end{bmatrix} \tag{2}$$

Journal of Information Systems Engineering and Management
2025, 10(4)
e-ISSN: 2468-4376
https://www.jisem-journal.com/

Research Article

where u_d and u_q represent the inverter input control voltages and K_p denotes the inverter gain. The inverter gain K_p is obtained from the DC-link voltage supplied to the inverter and the maximum control voltage, as [15]:

$$\boldsymbol{K_p = 0.65 \frac{V_{dc}}{V_{cm}}} \tag{3}$$

where V_{dc} is the DC voltage input to the inverter, and V_{cm} is the maximum control voltage.

The combination of IPMSM and inverter dynamics leads to the following relation.

$$\begin{aligned}
\boldsymbol{\frac{di_d}{dt}} &= \boldsymbol{-\frac{R_s}{L_d} i_d + n_p \frac{L_q}{L_d} i_q \omega_r + \frac{K_p}{L_d} u_d} \\
\boldsymbol{\frac{di_q}{dt}} &= \boldsymbol{-\frac{R_s}{L_q} i_q - n_p \frac{L_d}{L_q} i_d \omega_r - n_p \frac{\lambda_f}{L_q} \omega_r + \frac{K_p}{L_q} u_q} \\
\boldsymbol{\frac{d\omega_r}{dt}} &= \boldsymbol{\frac{3}{2} \frac{n_p}{J_m} \{\lambda_f i_q + (L_d - L_q) i_d i_q\} - \frac{B}{J_m} \omega_r - \frac{1}{J_m} T_L}
\end{aligned} \tag{4}$$

The proposed strategy adopts the constant torque angle operating scheme to ensure maximum torque production. This involves driving the d-axis current toward the zero-reference value, thereby directing the entire current to the q-axis. Therefore, the controlled output equation can be formulated as follows:

$$\boldsymbol{y} = \begin{bmatrix} i_d \\ \omega_r \end{bmatrix} \subset \mathbb{R}^2 \tag{5}$$

By selecting the state variable vector as $\boldsymbol{x} = [\, i_d \; i_q \; \omega_r \,]^T \in R^3$ and the input vector as $\boldsymbol{u} = [\, u_d \; u_q \,]^T \subset R^2$, the state space model of the IPMSM drive system can be reformulated as the following nonlinear model:

$$\begin{aligned}
\boldsymbol{\dot{x} = f(x, u, T_L)} &= \begin{bmatrix} \boldsymbol{\frac{1}{L_d}(-R_s x_1 + n_p L_q x_2 x_3 + K_p u_d)} \\ \boldsymbol{\frac{1}{L_q}(-n_p L_d x_1 x_3 - R_s x_2 - n_p \lambda_f x_3 + K_p u_q)} \\ \boldsymbol{\frac{K_t}{J_m \lambda_f}(L_d - L_q) x_1 x_2 + \frac{K_t}{J_m} x_2 - \frac{B}{J_m} x_3 - \left(\frac{1}{J_m}\right) T_L} \end{bmatrix} \\
\boldsymbol{y(t) = h(x)} &= \boldsymbol{\begin{bmatrix} 1 & 0 & 0 \\ 0 & 0 & 1 \end{bmatrix} \begin{bmatrix} x_1(t) \\ x_2(t) \\ x_3(t) \end{bmatrix}}
\end{aligned} \tag{6}$$

where $K_t = \frac{3}{2} n_p \lambda_f$ refers to the torque constant.

The dynamic model of the IPMSM described in the previous equation exhibits noticeable nonlinearities, as evidenced by the cross-coupling terms $(x_1 x_2)$ and $(x_1 x_3)$. Additionally, the system may face inevitable external disturbances, such as fluctuations in the applied load torque, which further complicate the control design.

The main design goals for the proposed control system are:

- Ensure the d-axis current accurately tracks the zero-reference level to produce optimal torque.
- Control the mechanical rotor speed to closely follow a time-varying reference speed profile, even during fluctuations in load torque.

Journal of Information Systems Engineering and Management
2025, 10(4)
e-ISSN: 2468-4376
https://www.jisem-journal.com/

Research Article

2.2 Linearized Model of an IPMSM under vector control

The approximation of the nonlinear dynamic model of IPMSM into a linear representation is a prerequisite for designing state feedback control. By using the Jacobian method [18], the first step in the process is to identify the steady-state operating point through solving the nonlinear equations under the equilibrium condition, as illustrated by the following equation:

$$\boldsymbol{f}(\boldsymbol{x}_{ss}, \boldsymbol{u}_{ss}, T_L) = 0 \tag{7}$$

According to the IPMSM dynamic model described in Equation (4), the following conditions are satisfied during steady-state operation.

$$i_{dss} = i_{dref} = 0\,;\ \omega_{rss} = \omega_{ref}\,;\ \ i_{qss} = i_{qref} = \frac{J_m}{K_t}\left[\frac{B}{J_m}\omega_{rss} + \frac{1}{J_m}\,T_L\right] = f\left(\omega_{ref}, T_L\right) = \frac{J_m}{K_t}\,d(t) \tag{8}$$

where ω_{ref} represents the reference rotor speed, which ranges from zero to the base speed, and $d(t)$ denotes lumped disturbances that include the friction force and external load disturbances. From the equation mentioned above, it is clear that the operating point varies dynamically in response to changes in the reference speed and load torque. Thus, it can be expressed as a function of these variables as follows:

$$\boldsymbol{x_{ss}}\left(\omega_{ref}, T_L\right) = \begin{bmatrix} 0 & \dfrac{J_m}{K_t}\,d(t) & \omega_{ref} \end{bmatrix}^T = \begin{bmatrix} 0 & f\left(\omega_{ref}, T_L\right) & \omega_{ref} \end{bmatrix}^T \tag{9}$$

To accommodate these changes effectively, it is necessary to choose these variables as scheduling parameters and formulate the operating point in a parameterized form. Let $\omega_{ref}(t)$ and $T_L(t)$ be defined as the scheduling variables $\rho_1(t)$ and $\rho_2(t)$, respectively, and vary within the following ranges:

$$\begin{aligned} \rho_1(t) &\in [0 \quad \omega_{base}] \\ \rho_2(t) &\in [0 \quad T_{rated}] \end{aligned} \tag{10}$$

Then, the scheduling variables can be represented in a vector form as follows:

$$\boldsymbol{\rho}(t) = [\rho_1(t) \quad \rho_2(t)]^T = [\omega_{ref}(t) \quad T_L(t)]^T \subset \mathbb{R}^2 \tag{11}$$

Therefore, the operating point can be reformulated in parameterized form as:

$$\boldsymbol{x_{ss}}\left(\boldsymbol{\rho}(t)\right) = \begin{bmatrix} 0 & f\left(\rho_1(t), \rho_2(t)\right) & \rho_2(t) \end{bmatrix}^T \tag{12}$$

The approximation of the IPMSM dynamic model at the operating point $\boldsymbol{x_{ss}}\left(\boldsymbol{\rho}(t)\right)$ yields a parameterized linear model, which can be expressed by the following relation.

$$\begin{aligned} \dot{\boldsymbol{x}}(t) &= \mathbf{A}\left(\boldsymbol{\rho}(t)\right)\boldsymbol{x}(t) + \mathbf{B}\boldsymbol{u}(t) + \mathbf{E}\,\rho_2(t) \\ \boldsymbol{y}(t) &= \mathbf{C}\boldsymbol{x}(t) \end{aligned} \tag{13}$$

where the matrices **A**, **B**, **E**, and **C** take the following forms:

$$\mathbf{A}\left(\boldsymbol{\rho}(t)\right) = \begin{bmatrix} -\dfrac{R_s}{L_d} & n_p\,\dfrac{L_q}{L_d}\rho_1(t) & n_p\left(\dfrac{L_q}{L_d}\right)\dfrac{[B\rho_1(t) + \rho_2(t)]}{K_t} \\ -n_p\,\dfrac{L_d}{L_q}\,\rho_1(t) & -\dfrac{R_s}{L_q} & -n_p\,\dfrac{\lambda_f}{L_q} \\ \dfrac{(L_d - L_q)}{J_m\lambda_f}[B\rho_1(t) + \rho_2(t)] & \dfrac{K_t}{J_m} & -\dfrac{B}{J_m} \end{bmatrix}, \mathbf{B} = \begin{bmatrix} \dfrac{K_p}{L_d} & 0 \\ 0 & \dfrac{K_p}{L_q} \\ 0 & 0 \end{bmatrix},$$

$$\mathbf{E} = -\begin{bmatrix} 0 & 0 & \dfrac{1}{J_m} \end{bmatrix}^T, \quad \boldsymbol{C} = \begin{bmatrix} 1 & 0 & 0 \\ 0 & 0 & 1 \end{bmatrix} \tag{14}$$

Journal of Information Systems Engineering and Management
2025, 10(4)
e-ISSN: 2468-4376
https://www.jisem-journal.com/

Research Article

3. COMPOSITE GAIN SCHEDULED CONTROL DESIGN

The proposed composite control strategy consists of two main parts. The first part includes a baseline controller that relies on integral state feedback control to achieve the desired tracking performance. It also integrates a gain scheduling mechanism to enhance adaptability to changing conditions. The second part involves a disturbance estimation technique based on ESO to estimate the lumped disturbances affecting the speed loop, thereby contributing to enhanced system robustness. The tracking and robustness requirements can be attained by designing the feedback baseline controller and the ESO-type observer separately and then integrating them within the same control structure. Figure 1 depicts the block diagram of the proposed composite control scheme in the rotor reference frame.

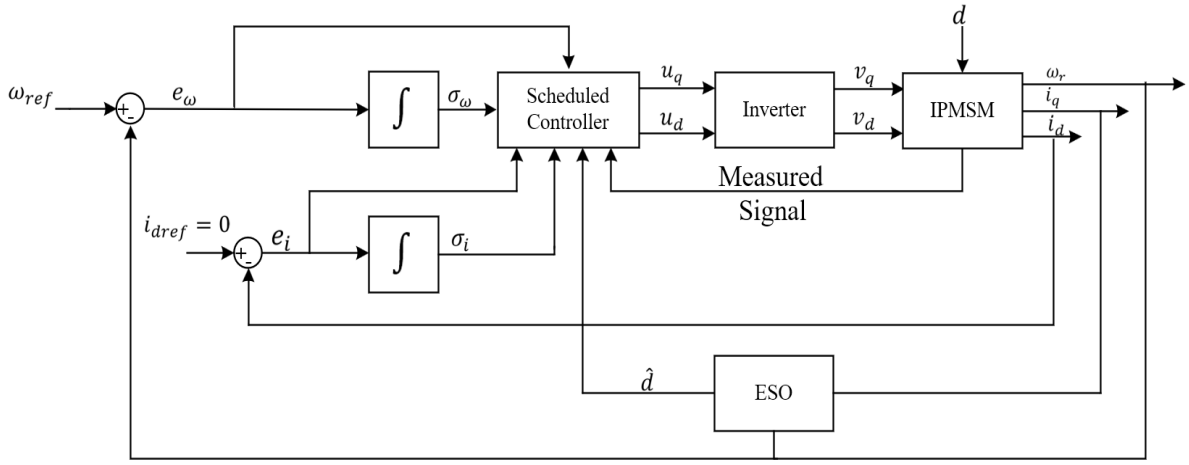

Figure 1. Block diagram of the proposed composite control scheme for IPMSM speed regulation

3.1 Extended State Observer Design

The design of ESO accounts for the mechanical dynamics of IPMSM. With the d-axis current maintained at a zero reference, the mechanical equation of motion simplifies to the following relation:

$$\frac{d\omega_r}{dt} = -\frac{B}{J_m}\omega_r - \frac{1}{J_m}T_L + \frac{K_t}{J_m}i_q \tag{15}$$

Since equation (8) defines the lumped disturbance in the following manner:

$$d(t) = -\frac{B}{J_m}\omega_r - \frac{1}{J_m}T_L \tag{16}$$

Then, the mechanical equation of motion can be reformulated as:

$$\frac{d\omega_r}{dt} = d(t) + b\, i_q \tag{17}$$

where $b = \frac{K_t}{J_m}$

Define $z_1 = \omega_r$, and $z_2 = d(t)$, then the equation above can be expressed in state space as:

$$\begin{aligned} \dot{\boldsymbol{z}} &= \mathbf{A}_z\boldsymbol{z}(t) + \mathbf{B}_z i_q(t) + \mathbf{E}_z\dot{d}(t) \\ \boldsymbol{y}_z &= \mathbf{C}_z\boldsymbol{z}(t) \end{aligned} \tag{18}$$

where

$$\mathbf{A}_z = \begin{bmatrix} 0 & 1 \\ 0 & 0 \end{bmatrix},\ \mathbf{B}_z = \begin{bmatrix} \boldsymbol{b} \\ \mathbf{0} \end{bmatrix},\ \mathbf{E}_z = \begin{bmatrix} 0 \\ 1 \end{bmatrix}, \text{ and } \mathbf{C}_z = [1 \quad 0].$$

Journal of Information Systems Engineering and Management
2025, 10(4)
e-ISSN: 2468-4376
https://www.jisem-journal.com/

Research Article

Based on the state space representation provided above, the structure of the second-order ESO is defined as follows:

$$\begin{bmatrix}\dot{\hat{z}}_1(t)\\ \dot{\hat{z}}_2(t)\end{bmatrix}=\begin{bmatrix}0 & 1\\ 0 & 0\end{bmatrix}\begin{bmatrix}\hat{z}_1(t)\\ \hat{z}_2(t)\end{bmatrix}+\begin{bmatrix}b\\ 0\end{bmatrix}i_q(t)+\begin{bmatrix}L_1\\ L_2\end{bmatrix}\left(y_z-\hat{y}_z(t)\right)$$
$$\hat{y}_z(t)=\begin{bmatrix}1 & 0\end{bmatrix}\begin{bmatrix}\hat{z}_1(t)\\ \hat{z}_2(t)\end{bmatrix} \quad (19)$$

where $\hat{z}_1(t)$ represents the estimated rotor speed ω_r, $\hat{z}_2(t)$, denoted as $\hat{d}(t)$, represents the estimate of the lumped disturbance $d(t)$, and L_1 and L_2 are the ESO observer feedback gains. Assuming that the lumped disturbance varies slowly and remains bounded, the following relation can be established:

$$\frac{d}{dt}d(t)\cong 0 \quad (20)$$

Define the estimation error state vector $\boldsymbol{e}_z(t)$ as:

$$\boldsymbol{e}_z(t)=\begin{bmatrix}e_{z1}(t)\\ e_{z1}(t)\end{bmatrix}=\begin{bmatrix}z_1(t)-\hat{z}_1(t)\\ z_2(t)-\hat{z}_2(t)\end{bmatrix} \quad (21)$$

The dynamics of observer error can be derived as follows:

$$\dot{\boldsymbol{e}}_z(t)=(\mathbf{A}_z-\boldsymbol{L}\mathbf{C}_z)\boldsymbol{e}_z(t) \quad (22)$$

If the feedback gain vector $\boldsymbol{L}=[L_1\ L_2\ ]^T$ is selected in such a way that the matrix $[\boldsymbol{A}_z-\boldsymbol{L}\boldsymbol{C}_z]$ is Hurwitz, then the estimation errors will converge to zero.

To simplify the tuning process of ESO gains, A bandwidth parameterization approach is utilized [19]. This approach allows for adjusting only a single parameter representing the desired ESO bandwidth (ω_0) rather than adjusting two separate gains. By setting the double poles of the ESO to the same position at $-\omega_0$, the ESO feedback gains can be determined by equating the following polynomial expressions:

$$\lambda(s)=s^2+L_1s+L_2=(s+\omega_0)^2 \quad (23)$$
$$\boldsymbol{L}=[L_1\quad L_2]^T=[2\omega_0\quad {\omega_0}^2]^T \quad (24)$$

According to equation (17), the reference q-axis current can be obtained from the estimated lumped disturbance $\hat{z}_2(t)$, as follows:

$$i_{qref}=-\frac{1}{b}\hat{z}_2(t)=-\frac{1}{b}\,\hat{d}(\mathrm{t}) \quad (25)$$

The estimated load torque can be obtained using the following formula:

$$\hat{T}_L=-B\hat{z}_1(t)-J_m\hat{z}_2(t)=-B\hat{z}_1(t)-J_m\hat{d}(\mathrm{t}) \quad (26)$$

Figure 2 illustrates the block diagram for obtaining the reference q-axis current using the ESO-type observer.

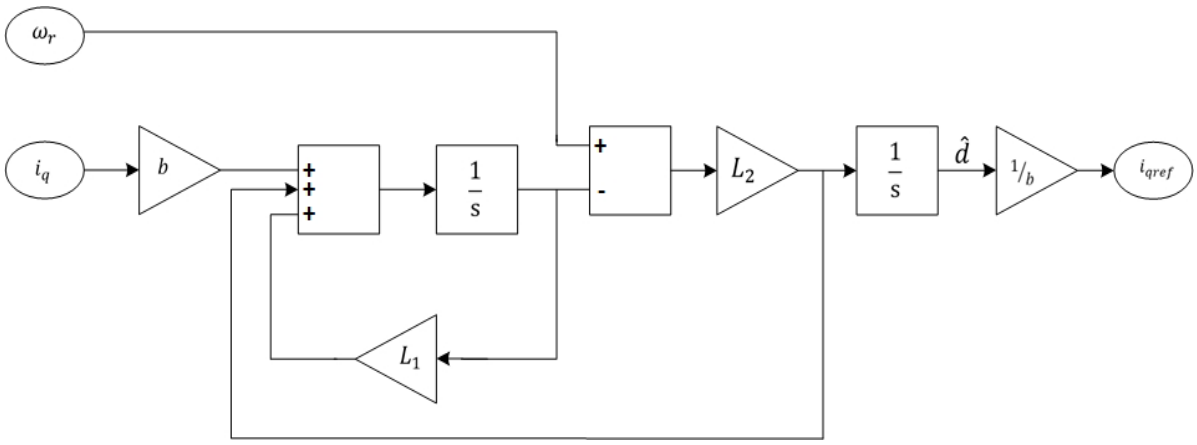

Figure 2. Block diagram of the 2nd-order Extended State Observer (ESO)

Journal of Information Systems Engineering and Management
2025, 10(4)
e-ISSN: 2468-4376
https://www.jisem-journal.com/

Research Article

3.2 Gain Scheduled Integral State Feedback Control Design for IPMSM

The gain-scheduling LQR control represents an enhanced version of fixed-gain LQR control, integrating an adaptive mechanism to manage dynamic changes. The adaptive feature arises from the iterative incorporation of the ESO disturbance estimates and the reference speed level into the linearized model, yielding dynamic updates in response to changing operating conditions. Consequently, the fixed-gain LQR transforms into a scheduled type, allowing for an automatic optimization process and adjustments to gain settings based on variations in load torque and reference speed, thereby ensuring optimal performance across different operating conditions. The control design begins with a fixed-gain approach, assuming a fixed operating point to simplify the design process. Once the initial design is complete, it transitions to a gain-scheduling framework by associating gain coefficients as functions of the scheduling variables.

The vector of reference inputs for d-axis current and rotor speed can be represented as:

$$\boldsymbol{r}(t) = \begin{bmatrix} i_{dref} \\ \omega_{ref} \end{bmatrix} = \begin{bmatrix} 0 \\ \text{desired speed} \end{bmatrix} \subset \mathbb{R}^2 \tag{27}$$

The proposed scheme includes two integral actions to achieve steady-state error-free control of the d-axis current and rotor speed. The vector of additional state variables can be written as:

$$\boldsymbol{\sigma}(t) = \begin{bmatrix} \sigma_1(t) \\ \sigma_2(t) \end{bmatrix} = \begin{bmatrix} \int (0 - i_d)dt \\ \int (\omega_{ref} - \omega_r)dt \end{bmatrix} \subset \mathbb{R}^2 \tag{28}$$

The state space equation of the integral actions can be expressed as:

$$\dot{\boldsymbol{\sigma}} = \boldsymbol{r} - \boldsymbol{y} = -\mathbf{C}\boldsymbol{x} + \boldsymbol{r} \tag{29}$$

By expanding the state vector to include the additional states, the state space equations of the augmented model can be written as:

$$\begin{bmatrix} \dot{\boldsymbol{x}}(t) \\ \dot{\boldsymbol{\sigma}}(t) \end{bmatrix} = \begin{bmatrix} \mathbf{A} & \mathbf{0} \\ -\mathbf{C} & \mathbf{0} \end{bmatrix} \begin{bmatrix} \boldsymbol{x}(t) \\ \boldsymbol{\sigma}(t) \end{bmatrix} + \begin{bmatrix} \mathbf{B} \\ \mathbf{0} \end{bmatrix} \boldsymbol{u}(t) + \begin{bmatrix} \mathbf{E} \\ \mathbf{0} \end{bmatrix} d + \begin{bmatrix} 0 \\ 1 \end{bmatrix} \omega_{ref}$$
$$\boldsymbol{y} = \begin{bmatrix} \mathbf{C} & \mathbf{0} \end{bmatrix} \begin{bmatrix} \boldsymbol{x}(t) \\ \boldsymbol{\sigma}(t) \end{bmatrix} \tag{30}$$

When the system reaches a steady state, the following equation applies:

$$\begin{bmatrix} \dot{\boldsymbol{x}}_{ss} \\ \dot{\boldsymbol{\sigma}}_{ss} \end{bmatrix} = \begin{bmatrix} \mathbf{A} & \mathbf{0} \\ -\mathbf{C} & \mathbf{0} \end{bmatrix} \begin{bmatrix} \boldsymbol{x}_{ss} \\ \boldsymbol{\sigma}_{ss} \end{bmatrix} + \begin{bmatrix} \mathbf{B} \\ \mathbf{0} \end{bmatrix} \boldsymbol{u}_{ss} + \begin{bmatrix} \mathbf{E} \\ \mathbf{0} \end{bmatrix} d + \begin{bmatrix} 0 \\ 1 \end{bmatrix} \omega_{ref} \tag{31}$$

Define

$$\begin{aligned} \boldsymbol{x}_e &= \boldsymbol{x}(t) - \boldsymbol{x}_{ss} \\ \boldsymbol{\sigma}_e &= \boldsymbol{\sigma}(t) - \boldsymbol{\sigma}_{ss} \\ \boldsymbol{u}_e &= \boldsymbol{u}(t) - \boldsymbol{u}_{ss} \end{aligned} \tag{32}$$

The error dynamic equation can be derived as:

$$\begin{bmatrix} \dot{\boldsymbol{x}}_e \\ \dot{\boldsymbol{\sigma}}_e \end{bmatrix} = \begin{bmatrix} \mathbf{A} & \mathbf{0} \\ -\mathbf{C} & \mathbf{0} \end{bmatrix} \begin{bmatrix} \boldsymbol{x}_e \\ \boldsymbol{\sigma}_e \end{bmatrix} + \begin{bmatrix} \mathbf{B} \\ \mathbf{0} \end{bmatrix} \boldsymbol{u}_e \tag{33}$$

Define a new error state vector $\boldsymbol{\eta}(t)$ by:

Journal of Information Systems Engineering and Management
2025, 10(4)
e-ISSN: 2468-4376
https://www.jisem-journal.com/

Research Article

$$\boldsymbol{\eta} = \begin{bmatrix} \boldsymbol{x}_e \\ \boldsymbol{\sigma}_e \end{bmatrix} \tag{34}$$

Then equation (33) becomes:

$$\dot{\boldsymbol{\eta}}(t) = \mathbf{A}_e \boldsymbol{\eta}(t) + \mathbf{B}_e \boldsymbol{u}_e(t) \tag{35}$$

where

$$\mathbf{A}_e = \begin{bmatrix} \mathbf{A} & \mathbf{0} \\ -\mathbf{C} & \mathbf{0} \end{bmatrix}, \mathbf{B}_e = \begin{bmatrix} \mathbf{B} \\ \mathbf{0} \end{bmatrix}$$

Provided that the state variables are available, the appropriate state feedback control adopts the following form:

$$\boldsymbol{u}_e(t) = -\mathbf{K}_e \boldsymbol{\eta}(t) = -\mathbf{K}_x \, \boldsymbol{x}_e + \mathbf{K}_\sigma \, \boldsymbol{\sigma}_e \tag{36}$$

where $\boldsymbol{K}_e = [\boldsymbol{K}_x \vdots -\boldsymbol{K}_\sigma]$ represent the gain matrix of the augmented model, and can be split into the gain matrix $\boldsymbol{K}_x$ for the original states and the gain matrix $\boldsymbol{K}_\sigma$ for the additional states. The substitution of control law (36) into equation (35) results in the following relation:

$$\dot{\boldsymbol{\eta}}(t) = [\mathbf{A}_e - \mathbf{B}_e \mathbf{K}_e] \, \boldsymbol{\eta}(t) \tag{37}$$

As demonstrated by equation (37), the tracking problem is reduced to determining the gain matrix $\boldsymbol{K}_e$ so that $[\mathbf{A}_e - \boldsymbol{B}_e \mathbf{K}_e]$ is a Hurwitz matrix, which guarantees the stability and convergence of the tracking error to zero.

When using the LQR method to determine the optimal gain matrix $\boldsymbol{K}_e$, The quadratic cost function that needs to be minimized is expressed as follows:

$$J(\boldsymbol{\eta}, \boldsymbol{u}) = \int_0^\infty (\boldsymbol{\eta}^T \mathbf{Q} \boldsymbol{\eta} + \boldsymbol{u}^T \mathbf{R} \boldsymbol{u}) \, dt \tag{38}$$

where $\boldsymbol{Q}$ and $\boldsymbol{R}$ represent symmetric positive semi-definite and positive definite penalty matrices of appropriate dimensions. The process of determining the optimal gain matrix involves formulating and solving the Riccati equation to obtain a positive definite matrix $\boldsymbol{P}$. The continuous-time Riccati equation is formulated as [20]:

$$\mathbf{A}_e^T \mathbf{P} + \mathbf{P} \mathbf{A}_e - \mathbf{P} \mathbf{B}_e \mathbf{R}^{-1} \mathbf{B}_e^T \mathbf{P} + \mathbf{Q} = \mathbf{0} \tag{39}$$

Once the matrix $\boldsymbol{P}$ is computed, the optimal gain matrix $\boldsymbol{K}_e$ can be determined using the following relation.

$$\mathbf{K}_e = \mathbf{R}^{-1} \mathbf{B}_e^T \mathbf{P} \tag{40}$$

The control system can evolve from the fixed-gain design structure to a scheduled version by relating the control parameters to the scheduling variables. The gain-scheduled control law can be expressed as follows:

$$\boldsymbol{u}(t) = -\mathbf{K}_e\left(\omega_{ref}, \hat{T}_L\right) \boldsymbol{\eta}(t) = -\mathbf{K}_\mathrm{x}\left(\omega_{ref}, \hat{T}_L\right) \, \boldsymbol{x}_e + \mathbf{K}_\sigma \left(\omega_{ref}, \hat{T}_L\right) \boldsymbol{\sigma}_e \tag{41}$$

where

$$\begin{aligned} \mathbf{K}_x \left(\omega_{ref}, \hat{T}_L\right) &= \begin{bmatrix} K_{x11}\left(\omega_{ref}, \hat{T}_L\right) & K_{x12}\left(\omega_{ref}, \hat{T}_L\right) & K_{x13}\left(\omega_{ref}, \hat{T}_L\right) \\ K_{x21}\left(\omega_{ref}, \hat{T}_L\right) & K_{x22}\left(\omega_{ref}, \hat{T}_L\right) & K_{x23}\left(\omega_{ref}, \hat{T}_L\right) \end{bmatrix} \\ \mathbf{K}_\sigma\left(\omega_{ref}, \hat{T}_L\right) &= \begin{bmatrix} K_{\sigma 11}\left(\omega_{ref}, \hat{T}_L\right) & K_{\sigma 12}\left(\omega_{ref}, \hat{T}_L\right) \\ K_{\sigma 21}\left(\omega_{ref}, \hat{T}_L\right) & K_{\sigma 22}\left(\omega_{ref}, \hat{T}_L\right) \end{bmatrix} \end{aligned} \tag{42}$$

Journal of Information Systems Engineering and Management
2025, 10(4)
e-ISSN: 2468-4376
https://www.jisem-journal.com/

Research Article

The gain-scheduled state feedback control law can be expressed in more detail as follows:

$$\boldsymbol{u}(t) = \begin{bmatrix} u_d \\ u_q \end{bmatrix} = \begin{bmatrix} K_{x11}(\omega_{ref}, \hat{T}_L) & K_{x12}(\omega_{ref}, \hat{T}_L) & K_{x13}(\omega_{ref}, \hat{T}_L) \\ K_{x21}(\omega_{ref}, \hat{T}_L) & K_{x22}(\omega_{ref}, \hat{T}_L) & K_{x23}(\omega_{ref}, \hat{T}_L) \end{bmatrix} \begin{bmatrix} i_d - 0 \\ i_q - i_{qref} \\ \omega_r - \omega_{ref} \end{bmatrix} + \begin{bmatrix} K_{\sigma 11}(\omega_{ref}, \hat{T}_L) & K_{\sigma 12}(\omega_{ref}, \hat{T}_L) \\ K_{\sigma 21}(\omega_{ref}, \hat{T}_L) & K_{\sigma 22}(\omega_{ref}, \hat{T}_L) \end{bmatrix} \begin{bmatrix} \int (0 - i_{ds})dt \\ \int (\omega_{ref} - \omega_r)dt \end{bmatrix} \quad (43)$$

4. SIMULATION AND RESULTS

Simulation tests were conducted in the MATLAB/Simulink environment to validate the effectiveness of the proposed scheduled control in accurately tracking the reference speed profile and mitigating the adverse effects of load disturbances. The performance of the scheduled LQR controller was compared to that of a fixed-gain LQR counterpart using metrics such as settling time, overshoot, speed deviation, and recovery time. Table 1 summarizes the basic parameters of the IPMSM motor used for the simulation tests [21].

Table 1: Basic parameters of the IPMSM motor system

Parameter	Symbols	Values
Rated torque	T_N	5 N.m
Rated speed	ω_N	1500 rpm
DC link voltage	V_{dc}	144 V
Pole pairs number	n_p	4
Stator Resistance	R_s	3.18 Ω
d-axis inductance	L_d	0.056 H
q-axis inductance	L_q	0.038 H
Moment of inertia	J_m	0.051 kg.m2
Rotor flux linkage	λ_f	0.42 Wb-turn
Viscous Friction Coefficient	B	0.071 N.m-s/rad

The simulation tests involved two scenarios representing different operating conditions. The first scenario dealt with tracking a step reference speed in the presence of sudden changes in load torque, while the second focused on following a time-varying reference speed profile under sudden changes in load torque.

For comparison purposes, the fixed-gain controller was designed for a specific operating point: a reference speed of 500 rpm and a load torque of 5 N·m. The gain matrices for the two control methods were obtained using the LQR command in MATLAB. The penalty matrices $\boldsymbol{Q}$ and $\boldsymbol{R}$ were adjusted through trial-and-error processes to optimize performance, leading to the following values:

$$\mathbf{Q} = \text{diag}\{50,5,5,7,10\}, \qquad \mathbf{R} = \text{diag}\{1,1\} \quad (44)$$

The ESO bandwidth for the scheduled control was set to 90 Hz to obtain a suitable trade-off between the rapid estimates and noise immunity.

4.1 Tracking performance under a step reference speed and load disturbances:

In this scenario, the performance of the scheduled controller in tracking a step reference speed under the presence of load disturbance was evaluated and compared to that of a fixed-gain counterpart. At the start of the simulation, the reference speed was set as a step change from 0 to 500 rpm and maintained at this level throughout the 10-second test. Figure 3 depicts the variable load torque profile assumed to be applied to the drive system to evaluate the robustness against sudden disturbances.

Journal of Information Systems Engineering and Management
2025, 10(4)
e-ISSN: 2468-4376
https://www.jisem-journal.com/

Research Article

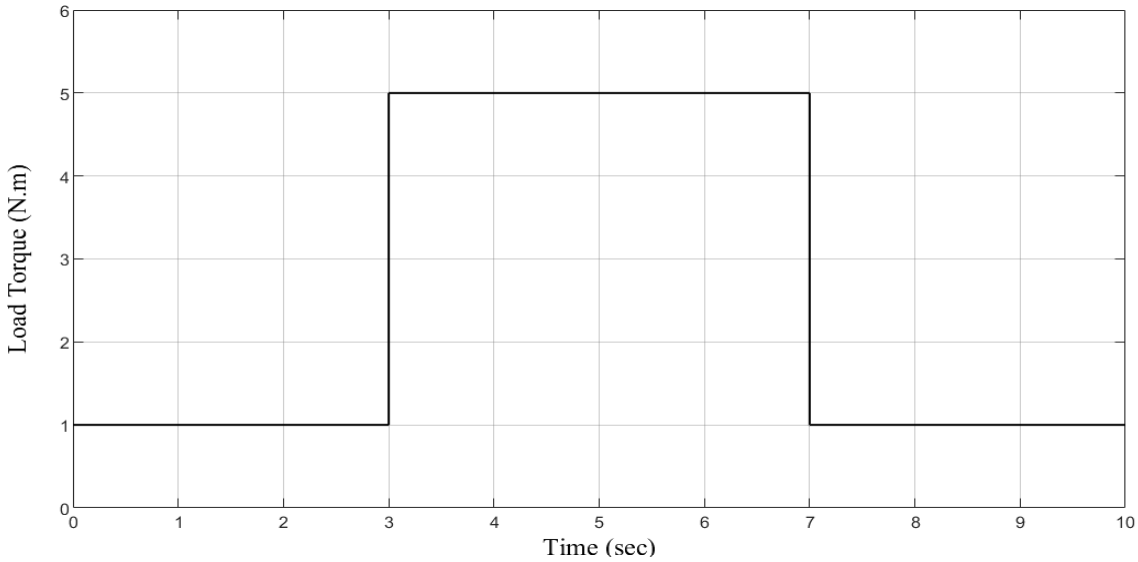

Figure 3. Load torque reference profile

Figure 4 depicts the step speed responses of both scheduled LQR control and fixed-gain LQR. The results indicate that the proposed scheduled controller outperforms the fixed-gain counterpart in terms of transient response and disturbance robustness.

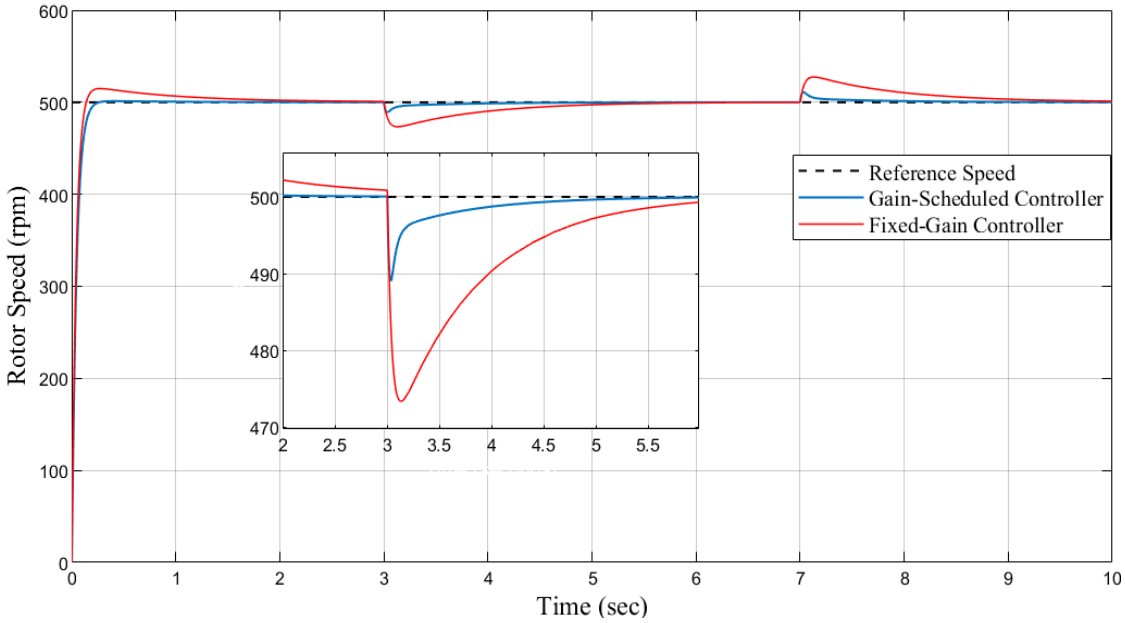

Figure 4. Comparison of rotor speed responses of the IPMSM control system under scheduled and fixed-gain controllers

In terms of transient performance, the scheduled controller achieves a much shorter settling time of 0.172 seconds compared to 0.89 seconds for the fixed-gain controller. Furthermore, the scheduled controller effectively drives the rotor speed to the reference level with negligible overshoot, while the fixed-gain controller produces 4% overshoot.

Regarding performance against external disturbances, the scheduled controller exhibits an enhanced capability to minimize speed deviations from the reference level, as evidenced by the speed deviations of 11 rpm (drop) and 11 rpm (rise) in response to sudden load application and removal, respectively, compared to 27 and 28 rpm with the fixed-gain controller. Additionally, the scheduled controller shows quicker restoration times of 0.05 seconds and 0.046

Journal of Information Systems Engineering and Management
2025, 10(4)
e-ISSN: 2468-4376
https://www.jisem-journal.com/

Research Article

seconds to recover from sudden load changes, unlike the slower recovery times of 0.97 seconds and 1.03 seconds exhibited by the fixed-gain controller.

Figure 5 shows the load torque estimates provided by the ESO observer. The results demonstrate its ability to track load changes and provide a rapid and accurate estimation of the applied load torque profile, thus facilitating the effective compensation for their effects.

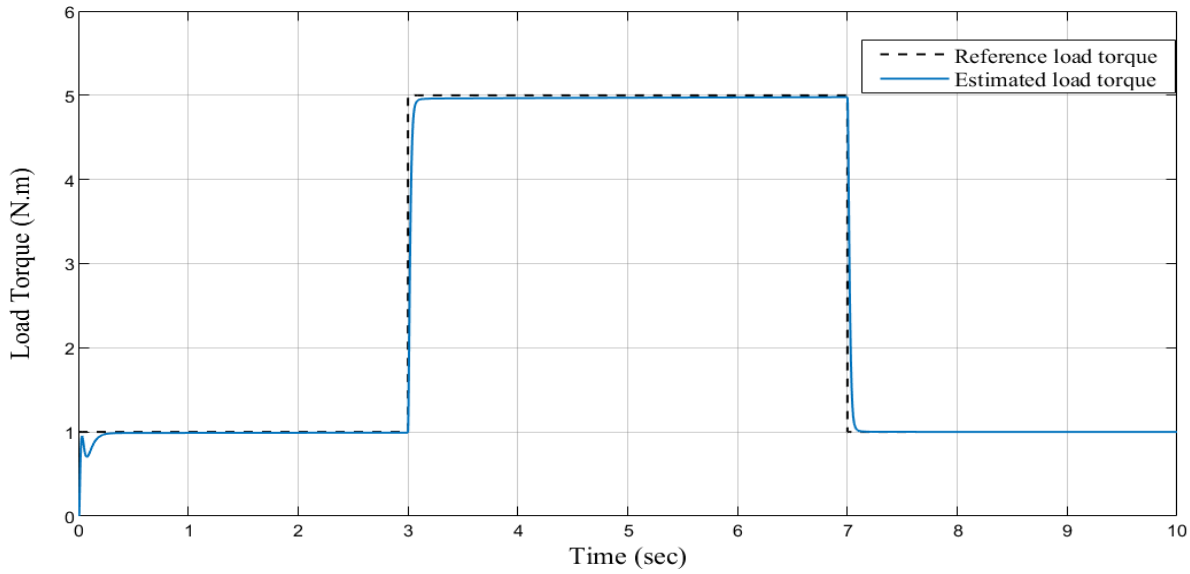

Figure 5. Time evolution of the reference and estimated load torque

To illustrate the differences in how each controller manages the q-axis current under sudden load changes. Figure 6 compares the q-axis current responses for the scheduled and fixed-gain controllers.

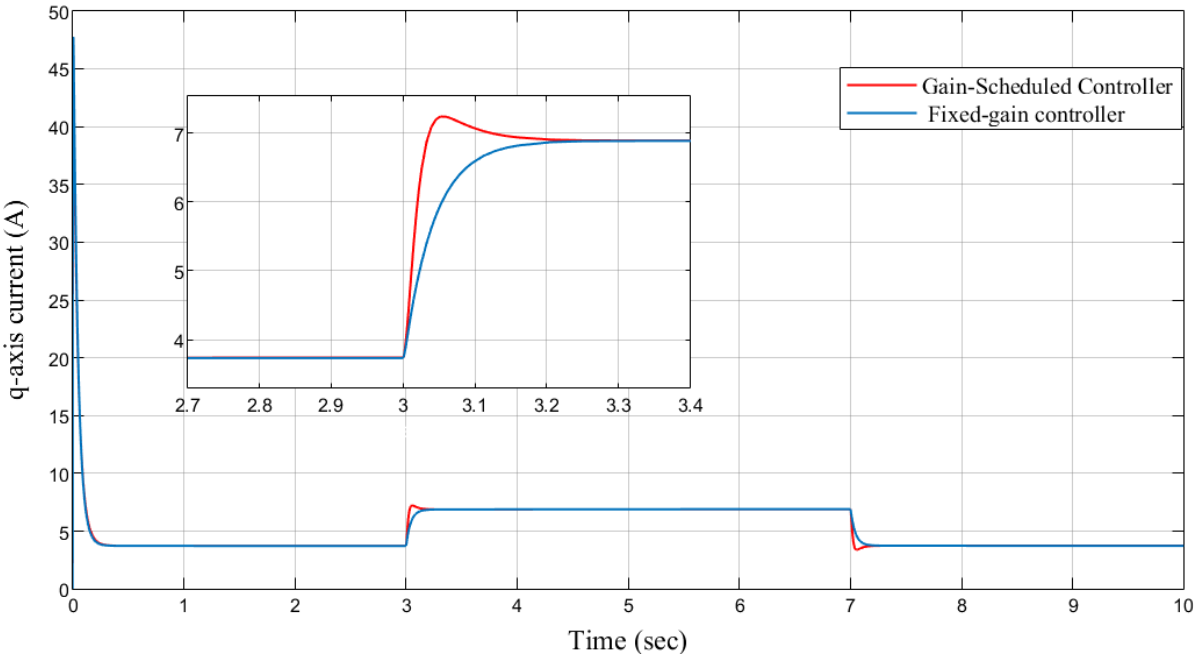

Figure 6. Response curves of q-axis current

The results show that the scheduled controller exhibits faster response and higher q-axis current under sudden load changes, resulting in increased torque production and rapid compensation for load disturbances. In contrast, the fixed-gain controller exhibits a more sluggish current response, leading to delayed compensation for load changes.

Journal of Information Systems Engineering and Management
2025, 10(4)
e-ISSN: 2468-4376
https://www.jisem-journal.com/

Research Article

Figure 7 shows the current responses along the d-axis for the scheduled and fixed-gain controllers. The results indicate that both controllers maintain the actual currents along the d-axis close to the zero reference, with minimal deviations due to load torque changes, unlike the q-axis currents, which demonstrate greater sensitivity to these changes. These results confirm the effectiveness of the decoupling feature provided by the applied vector control technique.

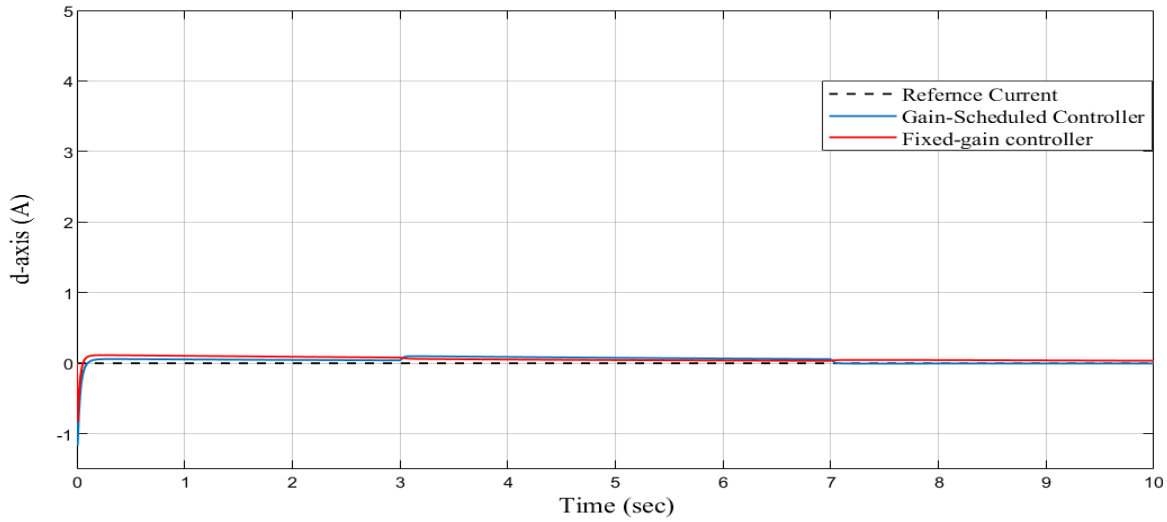

Figure 7. Response curves of d-axis current

4.2 Tracking performance under time-varying reference speed and load disturbances

The second test was conducted to verify the effectiveness of the scheduled control under more dynamic operating conditions compared to the first scenario. In this scenario, the reference speed was set as a ramp trajectory, accelerated from 0 to 1000 rpm over 10 seconds, using the same mechanical load torque profile employed in the previous scenario. Figure 8 depicts the speed responses of the IPMSM system under the control of the scheduled LQR controller and the fixed-gain LQR controller.

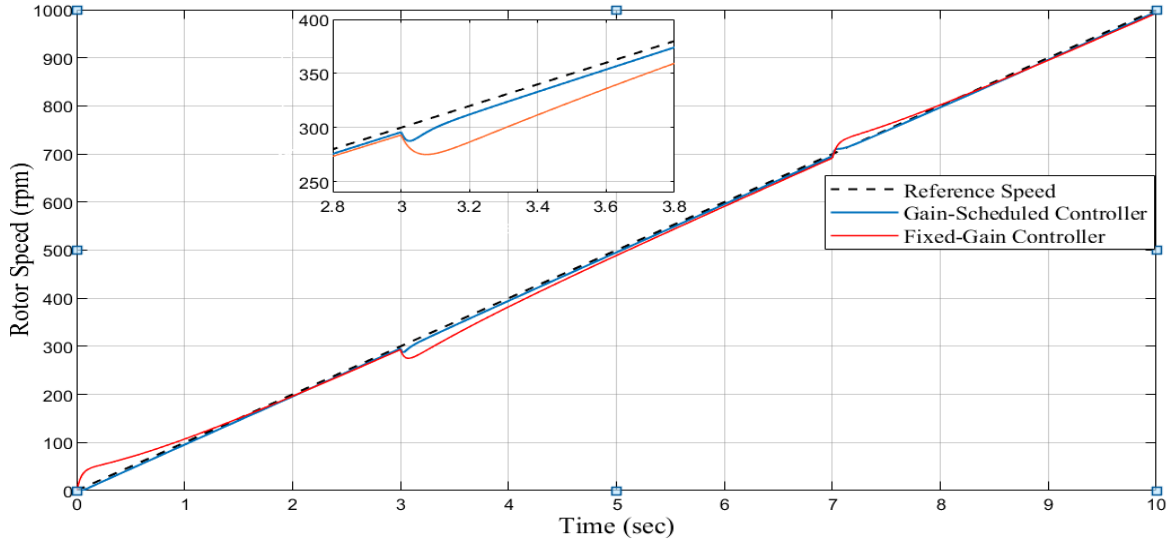

Figure 8. Speed responses of the IPMSM system under the scheduled and fixed-gain controllers

As illustrated in Figure 8, the scheduled control exhibits improved transient performance during the start-up phase, providing a smooth response with negligible overshoot and a near-instantaneous settling time. In contrast, the fixed-gain controller records significant overshoot and requires approximately 1.29 seconds to settle within 2% of the reference speed level.

Journal of Information Systems Engineering and Management
2025, 10(4)
e-ISSN: 2468-4376
https://www.jisem-journal.com/

Research Article

Moreover, the gain-scheduled controller exhibits strong robustness against load disturbances, recording lower speed deviations of 12 and 10 rpm compared to the 25 and 20 rpm observed by the fixed-gain controller. It also demonstrates faster restoring times, taking 0.15 and 0.08 seconds to recover from sudden load changes, compared to 1.1 and 0.4 seconds for the fixed-gain controller. These results indicate that the gain-scheduled controller can adjust to changing operating conditions and achieve enhanced tracking performance, even in the presence of sudden load disturbances.

Figure 9 illustrates the effectiveness of ESO in accurately estimating the applied external disturbance under time-varying speed conditions. It demonstrates rapid convergence towards the actual disturbance, enabling effective compensation for the disturbance's effects.

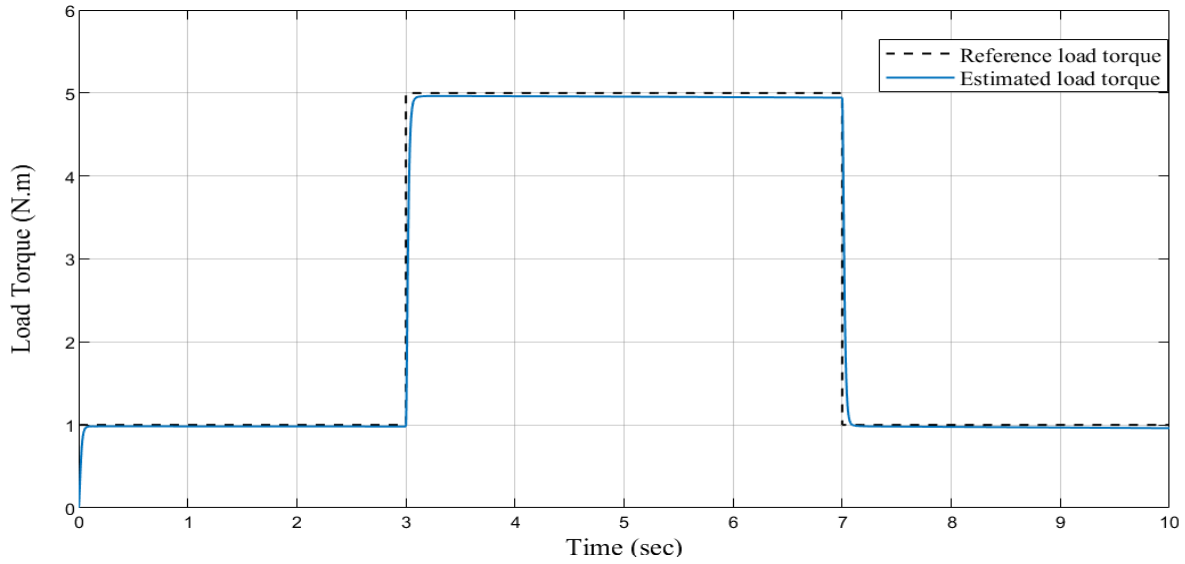

Figure 9. Time evolution of the reference and estimated load torque

Figure 10 compares the q-axis responses of the IPMSM system obtained using scheduled LQR and fixed gain controller techniques, illustrating how each controller reacts to sudden changes in the load torque.

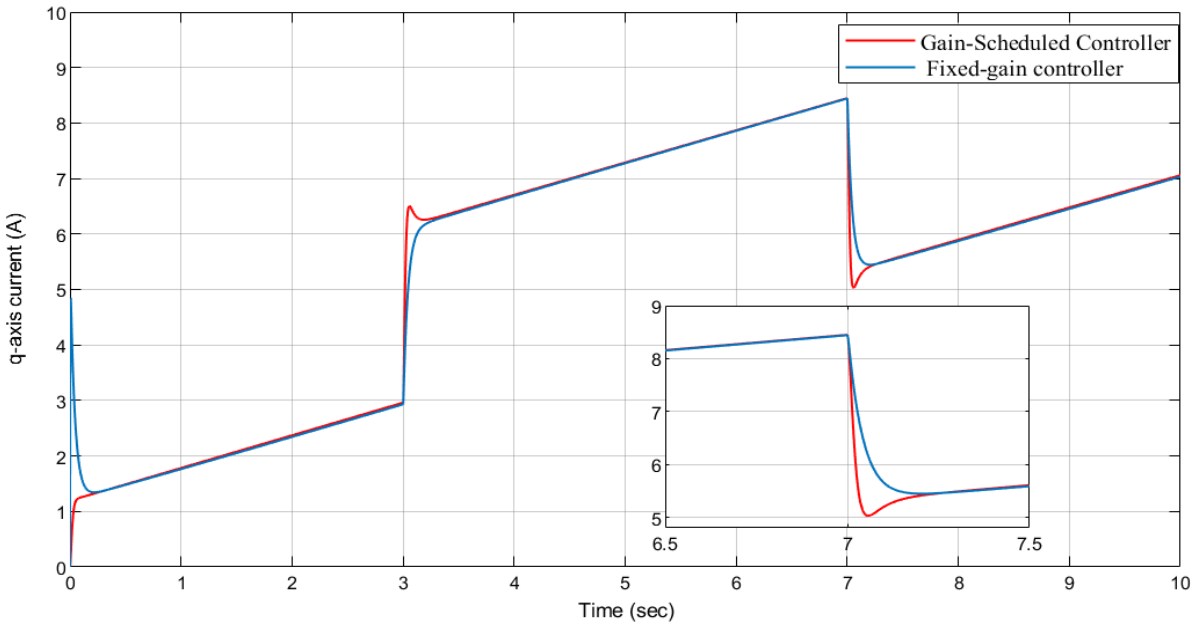

Figure 10. Response curves of q-axis current

Journal of Information Systems Engineering and Management
2025, 10(4)
e-ISSN: 2468-4376
https://www.jisem-journal.com/

Research Article

The results demonstrate that the fixed-gain controller cannot rapidly inject sufficient current into the q-axis to compensate for load disturbances. In contrast, the scheduled controller increases the current in the q-axis to generate more torque, allowing for rapid compensation of load changes.

Figure 11 displays the d-axis current responses of the IPMSM system under both scheduled control and fixed-gain control. The observation that both controllers maintain the d-axis currents near the zero references indicates that torque is generated primarily through the q-axis current.

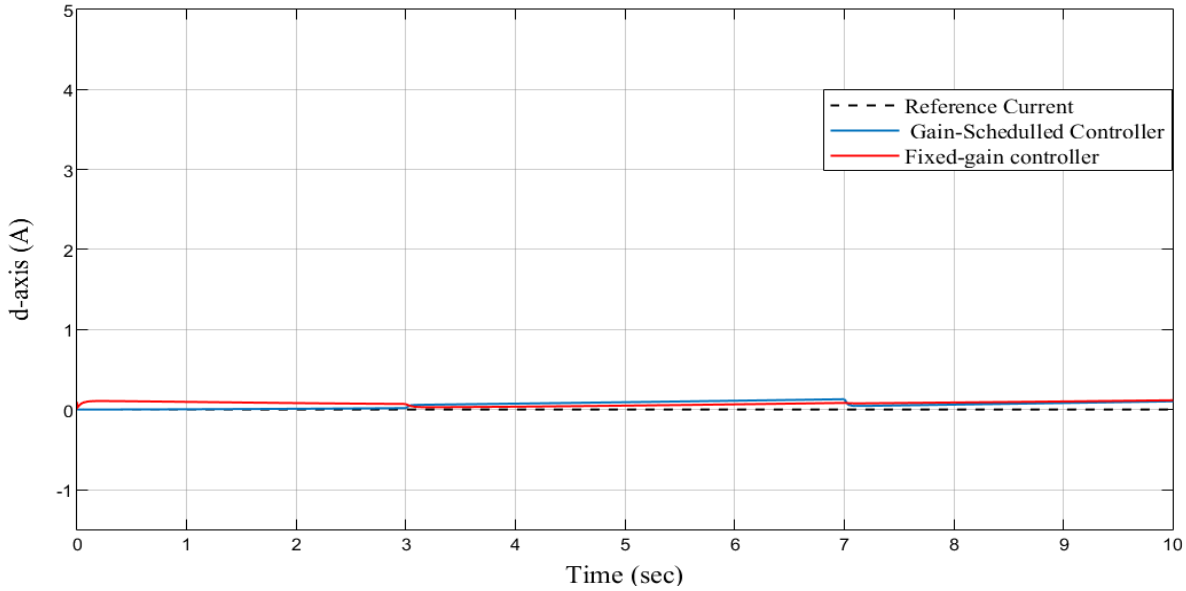

Figure 11. Response curves of d-axis current

4.3 Summary of results

Tables 2 and 3 summarize the key performance metrics obtained from the two test scenarios, highlighting the significant improvements that the suggested scheduled control offers over its fixed-gain counterpart, particularly in dynamic response and robustness against disturbances.

Table 2. Summary of performance metrics in the first testing scenario.

Performance indices	Fixed-Gain Controller	Scheduled-Gain Controller
Settling Time (s)	0.89	0.172
Overshoot (%)	4	0.2
Max speed deviation (rpm)	28	11
Max Recovery Time (s)	1.03	0.05

Table 3. Summary of performance metrics in the second testing scenario

Performance indices	Fixed-Gain Controller	Scheduled-Gain Controller
Settling Time (s)	1.29	0
Overshoot (%)	350	0
Max speed deviation (rpm)	25	12
Max Recovery Time (s)	1.1	0.15

The improved performance achieved by the scheduled control is attributed to the automated modification of the control law according to reference speed levels and the accurate estimates provided by the ESO. In contrast, the limited adaptability and robustness demonstrated by the fixed-gain control arise from its reliance on integral action

alone to compensate for speed errors and disturbances, slowing down the speed of dynamic response and consequently resulting in performance degradation.

5. CONCLUSION

The paper introduced the design of a composite scheduled control approach that employs LQR as a feedback controller and an ESO-type observer for estimating disturbances, while integrating a scheduling mechanism to enhance the anti-disturbance and tracking performance of the IPMSM under varying operating conditions. The ESO was designed based on the mechanical dynamics of the IPMSM and integrated into the speed control loop to estimate the lumped disturbance affecting the loop. The dynamic model of the IPMSM was developed in the rotor reference frame and approximated as a parameterized linear formulation to accommodate changes in linear dynamics. The approximated model was then regulated using integral state feedback control integrated with a gain scheduling framework. Based on the reference speed level and disturbance estimates provided by the ESO, the scheduled controller consistently adjusted the parameters of the linearized model and updated the control law to adapt to changes in operating conditions. The effectiveness of the proposed control strategy was validated through simulation tests in the MATLAB/Simulink environment. The results indicated that the scheduled controller outperformed its fixed-gain counterpart in dynamic tracking performance and robustness against disturbances. Further research will focus on creating sensorless configurations and employing field-weakening operating strategies to extend the speed range beyond base speed, thus broadening the application scope in more complex and dynamic environments.

REFERENCES

[1.] M. S. Rafaq and J.-W. Jung, "A comprehensive review of state-of-the-art parameter estimation techniques for permanent magnet synchronous motors in wide speed range," *IEEE Trans. Ind. Informat.*, vol. 16, no. 7, pp. 4747–4758, Jul. 2020, doi: 10.1109/TII.2019.2944413.

[2.] M. Monadi, M. Nabipour, F. Akbari-Behbahani, and E. Pouresmaeil, "Speed control techniques for permanent magnet synchronous motors in electric vehicle applications towards sustainable energy mobility: A review," *IEEE Access*, vol. 12, pp. 119615–119632, Aug. 2024, doi: 10.1109/ACCESS.2024.3450199.

[3.] Y. Ma and Y. Li, "Active disturbance compensation based robust control for speed regulation system of permanent magnet synchronous motor," *Appl. Sci.*, vol. 10, no. 2, Art. 709, Jan. 2020, doi: 10.3390/app10020709.

[4.] S. Tasouijan, J. Lee, K. Grigoriadis, and M. Franchek, "Robust linear parameter-varying output-feedback control of permanent magnet synchronous motors," *Syst. Sci. Control Eng.*, vol. 9, no. 1, pp. 612–622, Sep. 2021, doi: 10.1080/21642583.2021.1974600.

[5.] C. I. Nicola, M. Nicola, and D. Selișteanu, "Sensorless control of PMSM based on backstepping-PSO-type controller and ESO-type observer using real-time hardware," *Electronics*, vol. 10, no. 17, Art. 2080, Aug. 2021, doi: 10.3390/electronics10172080.

[6.] J. Qian, C. Ji, N. Pan, and J. Wu, "Improved sliding mode control for permanent magnet synchronous motor speed regulation system," *Appl. Sci.*, vol. 8, no. 12, Art. 2491, Dec. 2018, doi: 10.3390/app8122491.

[7.] L. Qu, W. Qiao, and L. Qu, "An extended-state-observer-based sliding-mode speed control for permanent-magnet synchronous motors," *IEEE J. Emerg. Sel. Topics Power Electron.*, vol. 9, no. 2, pp. 1605–1613, Apr. 2021, doi: 10.1109/JESTPE.2020.2990442.

[8.] J. Yang, W.-H. Chen, S. Li, L. Guo, and Y. Yan, "Disturbance/uncertainty estimation and attenuation techniques in PMSM drives—A survey," *IEEE Trans. Ind. Electron.*, vol. 64, no. 4, pp. 3273–3285, Apr. 2017, doi: 10.1109/TIE.2016.2583412.

[9.] W.-H. Chen, J. Yang, L. Guo, and S. Li, "Disturbance-observer-based control and related methods—An overview," *IEEE Trans. Ind. Electron.*, vol. 63, no. 2, pp. 1083–1095, Feb. 2016, doi: 10.1109/TIE.2015.2478397.

Research Article

[10.] Y. Fang, H. Kong, and T. Liu, "Nonlinear disturbance observer-based sliding mode control for the PMSM with matched and mismatched disturbances," *Math. Probl. Eng.*, vol. 2020, Art. 8837101, Dec. 2020, doi: 10.1155/2020/8837101.

[11.] Y. H. Lan and Lei-Zhou, "Backstepping control with disturbance observer for permanent magnet synchronous motor," *J. Control Sci. Eng.*, vol. 2018, Art. 4938389, Jul. 2018, doi: 10.1155/2018/4938389.

[12.] P. Chen and Y. Luo, "A two-degree-of-freedom controller design satisfying separation principle with fractional-order PD and generalized ESO," *IEEE/ASME Trans. Mechatronics*, vol. 27, no. 1, pp. 137–148, Feb. 2022, doi: 10.1109/TMECH.2021.3059160.

[13.] S. Li, J. Xu, S. Yuan, J. Li, and H. Sun, "Composite anti-disturbance control of permanent magnet synchronous motor based on feedback linearization," in *Proc. 8th IEEE Annu. Int. Conf. CYBER Technol. Autom., Control, Intell. Syst.*, Tianjin, China, Jul. 2018, pp. 1237–1242, doi: 10.1109/CYBER.2018.8688298.

[14.] BBBA. Apte, V. A. Joshi, H. Mehta, and R. Walambe, "Disturbance-observer-based sensorless control of PMSM using integral state feedback controller," *IEEE Trans. Power Electron.*, vol. 35, no. 6, pp. 6082–6090, Jun. 2020, doi: 10.1109/TPEL.2019.2949921.

[15.] R. Krishnan, *Permanent Magnet Synchronous and Brushless DC Motor Drives*. Boca Raton, FL, USA: CRC Press, 2010.

[16.] L. M. Grzesiak and T. Tarczewski, "Permanent magnet synchronous motor discrete linear quadratic speed controller," in *Proc. IEEE Int. Symp. Ind. Electron.*, Gdansk, Poland, Jun. 2011, pp. 667–672, doi: 10.1109/ISIE.2011.5984237.

[17.] T. Tarczewski and L. M. Grzesiak, "Constrained state feedback speed control of PMSM based on model predictive approach," *IEEE Trans. Ind. Electron.*, vol. 63, no. 6, pp. 3867–3875, Jun. 2016, doi: 10.1109/TIE.2015.2497302.

[18.] H. K. Khalil, *Nonlinear Systems*, 3rd ed. Upper Saddle River, NJ, USA: Prentice Hall, 2002.

[19.] Z. Gao, "Scaling and bandwidth-parameterization based controller tuning," in *Proc. Amer. Control Conf.*, Denver, CO, USA, Jun. 2003, pp. 4989–4996, doi: 10.1109/ACC.2003.1242516.

[20.] K. Ogata, *Modern Control Engineering*, 5th ed. Upper Saddle River, NJ, USA: Prentice Hall, 2010.

[21.] C. Sain, A. Banerjee, and P. K. Biswas, *Control Strategies of Permanent Magnet Synchronous Motor Drive for Electric Vehicles*. Boca Raton, FL, USA: CRC Press, 2022.